Swelling of nuclei embedded in neutron-gas and consequences for fusion

A. S. Umar, V. E. Oberacker, C. J. Horowitz, P.-G. Reinhard, and J. A. Maruhn

Swelling of nuclei embedded in neutron-gas and consequences for fusion

A.S. Umar,[1, *] V.E. Oberacker,[1, †] C. J. Horowitz,[2, ‡] P.-G. Reinhard,[3, §] and J.A. Maruhn[4, ¶]

[1]*Department of Physics and Astronomy, Vanderbilt University, Nashville, TN 37235, USA*
[2]*Department of Physics and CEEM, Indiana University, Bloomington, IN 47405, USA*
[3]*Institut für Theoretische Physik, Universität Erlangen, D-91054 Erlangen, Germany*
[4]*Institut für Theoretische Physik, Goethe-Universität, D-60438 Frankfurt am Main, Germany*

Fusion of very neutron rich nuclei may be important to determine the composition and heating of the crust of accreting neutron stars. We present an exploratory study of the effect of the neutron-gas environment on the structure of nuclei and the consequences for pycnonuclear fusion cross-sections in the neutron drip region. We studied the formation and properties of Oxygen and Calcium isotopes embedded in varying neutron-gas densities. We observe that the formed isotope is the drip-line nucleus for the given effective interaction. Increasing the neutron-gas density leads to the swelling of the nuclear density. We have used these densities to study the effect of this swelling on the fusion cross-sections using the São-Paulo potential. At high neutron-gas densities the cross-section is substantially increased but at lower densities the modification is minimal.

I. INTRODUCTION

Recent advances in radioactive beam technologies have opened up new experimental possibilities to study fusion of neutron rich nuclei [1]. Furthermore, near barrier fusion cross sections are relatively large so experiments are feasible with modest beam intensities. In addition, measurements are possible at the TRIUMF ISAC facility and in the near future at the NSCL ReA3-6 reaccelerated beam facility. Other radioactive ion beam facilities include ATLAS-CARIBU at Argonne National Laboratory, SPIRAL2 at GANIL (France), and RIBF at RIKEN (Japan). Note that the dynamics of the neutron rich skin of these nuclei can enhance the cross-section over that predicted by a simple static barrier penetration model. For example, neutrons may be transferred from the neutron rich beam to the stable target. Fusion of very neutron rich nuclei, near the drip line, raise very interesting nuclear structure and nuclear dynamics questions.

Neutron stars, in binary systems, can accrete material from their companions. This material undergoes a variety of nuclear reactions [2]. First at low densities, conventional thermonuclear fusion takes place, see for example [3]. Next at higher densities, the rising electron Fermi energy induces a series of electron captures [4] to produce increasingly neutron rich nuclei. Finally at high densities, these very neutron rich nuclei can fuse via pycnonuclear reactions. Pycnonuclear fusion is induced by quantum zero point motion [5, 6]. The energy released, and the densities at which these reactions occur, are important for determining the temperature and composition profile of accreting neutron star crusts. The existence of the inner neutron-star crust, in which very neutron rich nuclei are immersed in a gas of neutrons raises the question, what is the impact of this neutron gas on nuclear fusion rates? This neutron drip region is believed to occur for densities in the approximate range of a few $\times 10^{11}$ to 8×10^{13} g/cm^3. One of the early studies of the inner crust, consisting of drip-line nuclei combined with the background neutron gas, had been done by Negele and Vautherin [7]. Therefore understanding fusion reactions of neutron rich isotopes near the drip line are important. Horowitz *et al.* [8] calculate the enhancement in fusion rates from strong ion screening using molecular dynamics simulations, and find that ^{24}O + ^{24}O can fuse near 10^{11} g/cm^3, just before neutron drip. Extensive studies of the astrophysical $S(E)$ factors have been done using densities emanating from microscopic calculations and a barrier penetration model for fusion [9, 10]. Furthermore, this fusion can take place in the background neutron gas that is present in the inner crust of a neutron star. The possible effect of the neutron gas background was discussed in Ref. [10] by empirically changing the barrier height and width. Here, we study this effect by considering the presence of the background neutron gas microscopically by directly including the neutron gas and the nucleus in the same framework. We explicitly calculate the self-consistent proton and neutron densities of a single nucleus in equilibrium with the background neutron gas. Furthermore, for astrophysical applications, it seems clear that this adiabatic approach is the one that is relevant for calculating fusion rates in the inner crust. The neutron gas should have plenty of time to adjust to the presence of a nucleus.

The paper is organized as follows. Our computational approach to consider the presence of neutron gas together with the nucleus and the model for calculating the fusion cross-sections is discussed in Sec. II. Computational results for the Oxygen and Calcium systems is described in Sec. III. Finally, these results are discussed and we conclude in Sec. IV.

---

* umar@compsci.cas.vanderbilt.edu
† volker.e.oberacker@vanderbilt.edu
‡ horowit@indiana.edu
§ paul-gerhard.reinhard@physik.uni-erlangen.de
¶ maruhn@th.physik.uni-frankfurt.de

II. COMPUTATIONAL DETAILS

A. Computational setup

Hartree-Fock (HF) calculations were done in a three-dimensional Cartesian geometry with no symmetry assumptions and using the Skyrme effective nucleon-nucleon interaction [11]. The infinite neutron star crust environment is simulated by using a three-dimensional Cartesian box with periodic boundary conditions for both the bound and neutron gas states as well as the solution of the Poisson equation for the Coulomb potential, which is performed using Fast-Fourier Transform (FFT) techniques [12]. The Coulomb solution assumes global neutrality which means that the proton charges are compensated by a homogeneous negative electron gas cloud. In practice, this is achieved by setting the zero-momentum part of the Coulomb field in Fourier space to zero. The code uses the basis-spline collocation method for the lattice discretization of the HF equations using periodic boundary-conditions as described in Refs. [13–15]. The HF equations are solved using the damped gradient iteration method. The Skyrme parametrization used was SLy4 [16]. In addition to providing a good description of nuclei this interaction has been used to produce an equation of state for neutron stars [17].

For the choice of initial states to be used in HF minimization we have tried a number of choices, which all resulted in the same identical solution. One can first generate any isotope of the desired nucleus by solving the HF equations as described above and subsequently combine these states with a large number of free neutron gas states and minimize the entire system again. Alternately, one can simply choose a number of free proton states together with a large number of free neutron states and minimize this system. Both methods result in exactly the same numerical solution with a drip-line isotope corresponding to the nucleus with the given number of protons embedded in a given density of neutron gas states. Initial states, ψ, are spinors with a non-zero upper component in case of time-reversal invariance. In case of no time-reversal invariance the number of states are doubled by adding spinors having non-zero lower components as well. They satisfy the periodicity condition

$$\psi_{\mathbf{n}}(\mathbf{r} + \mathbf{L}) = \psi_{\mathbf{n}}(\mathbf{r}) , \qquad (1)$$

where $\mathbf{n} = (n_x, n_y, n_z)$ and n_a taking on integer values $-N_a, \ldots, +N_a$. Free states satisfying the above periodicity condition are simple plane-wave states with the appropriate normalization

$$\psi_{\mathbf{n}}(\mathbf{r}) = \frac{1}{\sqrt{L_x L_y L_z}} e^{i(k_{n_x} x + k_{n_y} y + k_{n_z} z)} \chi_n , \qquad (2)$$

where $k_{n_a} = 2\pi n_a / L_a$ and χ_n is an up or down spinor. The initial neutron and proton densities are perfectly uniform filling the entire numerical box. These initial states comprise the total number of states used in the

self-consistent HF problem using the Skyrme interaction. For even number of states time-reversal is valid and the HF single-particle Hamiltonian only depends on particle density, ρ, kinetic energy density. τ, and the spin-orbit pseudotensor $\mathbf{J}$ through the single-particle states [16]

$$\mathbf{h}\left(\{\phi_\mu\}\right) \phi_\lambda = \epsilon_\lambda \phi_\lambda \qquad \lambda = 1, ..., N . \qquad (3)$$

As the HF iterations proceed (preserving orthogonality for the entire system) some states evolve to form a bound nuclear system while the others remain as gas states showing some non-uniformity due to the presence of shell effects.

B. Fusion cross-sections

The São Paulo model of fusion calculates an effective nuclear potential based on the density overlap between colliding nuclei [18, 19]. Sub-barrier fusion cross-sections can then be calculated via tunneling. The model can be easily applied to a very large range of fusion reactions and qualitatively reproduces many experimental cross-sections [20, 21]. Recently this model was used to tabulate astrophysical S factors describing fusion of many carbon, oxygen, neon and magnesium isotopes for use in astrophysical simulations [9], see also Ref. [22].

In this section we describe the São Paulo barrier penetration model to calculate fusion cross-sections. This starts with the double folding potential $V_F(R)$ [18, 19],

$$V_F(R) = \int d^3 r_1 d^3 r_2 \rho_1(r_1) \rho_2(r_2) V_0 \delta(\mathbf{r}_1 - \mathbf{r}_2 - \mathbf{R}) . \quad (4)$$

Here ρ_1 and ρ_2 are the densities of the two nuclei and $V_0 = -450$ MeV-fm^3. From V_F a nonlocal potential $V_N(R, E)$ is constructed, $V_N(R, E) = V_F(R) e^{-4v^2/c^2}$, where v is the local relative velocity [18, 19] between the two nuclei at separation R (c is the speed of light)

$$v^2(R, E) = \frac{2}{\mu} \left[E - V_C(R) - V_N(R, E) \right] . \qquad (5)$$

Here μ is the reduced mass and $V_C(R)$ is the Coulomb potential at R. In practice, we use FFT techniques to calculate $V_F(R)$ as well as the Coulomb potential $V_C(R)$ (instead of using the point Coulomb formula). The velocity equation (5) has to be solved by iteration at each value of R and E.

Note that the neutron gas background could behave differently for two nuclei in close proximity then it does for only a single nucleus. However for simplicity, in this first study, we consider only a single nucleus in the background gas at a time in order to get the density profiles shown in Fig. 2. We then use these profiles in Eq. 4 and assume they are unmodified by the presence of the second nucleus.

The fusion barrier penetrabilities $T_L(E_{\text{c.m.}})$ are obtained by numerical integration of the two-body

Schrödinger equation

$$\left[\frac{-\hbar^2}{2\mu}\frac{d^2}{dR^2} + \frac{L(L+1)\hbar^2}{2\mu R^2} + V(R,E) - E\right]\psi = 0 \ , \quad (6)$$

using the *incoming wave boundary condition* (IWBC) method [23]. The potential $V(R,E)$ is the sum of nuclear and Coulomb potentials. IWBC assumes that once the minimum of the potential is reached fusion will occur. In practice, the Schrödinger equation is integrated from the potential minimum, $R_{\min}$, where only an incoming wave is assumed, to a large asymptotic distance, where it is matched to incoming and outgoing Coulomb wavefunctions. The barrier penetration factor, $T_L(E_{\rm c.m.})$ is the ratio of the incoming flux at $R_{\min}$ to the incoming Coulomb flux at large distance. Here, we implement the IWBC method exactly as it is formulated for the coupled-channel code CCFULL described in Ref. [23]. This gives us a consistent way for calculating cross-sections at above and below the barrier via

$$\sigma_f(E_{\rm c.m.}) = \frac{\pi}{k^2}\sum_{L=0}^{\infty}(2L+1)T_L(E_{\rm c.m.}) \ . \quad (7)$$

III. RESULTS

All the calculations presented here were done using a three-dimensional cubic Cartesian box with 31 fm sides and 1.0 fm lattice spacing. With the basis-spline method this gives highly accurate results for the HF problem [13]. We studied two systems with $Z = 8$ and $Z = 20$ protons inside a neutron gas. The resulting nuclei are always spherical and density profiles can be obtained by taking a cut along a particular axis. Our mesh includes the origin in all directions. We have repeated some of these calculations in a cubic bot with 41 fm sides and for the same neutron-gas density the results were numerically indistinguishable.

A. $Z = 8$ system

In these calculations we start with 8 proton states and a number of neutron states ranging from $50 - 1020$. The Skyrme SLy4 force gives ^{28}O as the slightly bound dripline nucleus in free-space. For the above range of neutron states we also find the ^{28}O to be the bound part of the system. As the number of neutron states is increased an overall negative potential is developed permeating the entire box. Figure 1 shows the neutron and proton mean-field potentials (solid lines) for $Z = 8$ and 520 neutrons. The dashed lines indicate the energies of the bound single-particle states with degeneracies shown in brackets. We define $N_{\rm bound}$ as the highest neutron s.p. state below the continuum threshold. Consequently, the
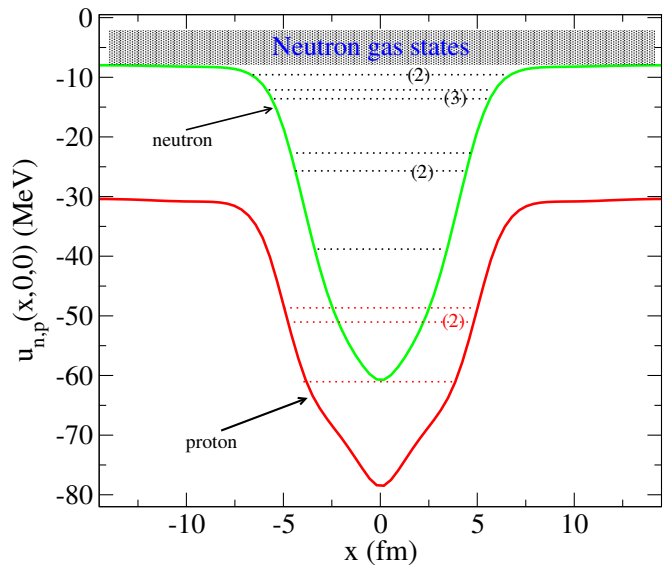

FIG. 1. (Color online) Mean-field potentials for neutrons and protons (solid lines) for the system with $Z = 8$ and 520 neutrons. The dashed lines indicate the energies of the bound single-particle states with degeneracies shown in brackets.

bound and gas densities become

$$\rho_{\rm bound} = \sum_{\lambda=1}^{N_{\rm bound}}|\phi_\lambda|^2 \ , \quad (8)$$

$$\rho_{\rm free} = \sum_{\lambda > N_{\rm bound}}|\phi_\lambda|^2 \ . \quad (9)$$

In this case the asymptotic value of the neutron potential is about -8 MeV. As it is the case in free-space increasing neutron number leads to deepening of the proton potential. In Fig. 2 we show the density profiles for neutrons and protons as well as the total density as a function of the number of neutron-gas states. The top frame shows the total density behavior as the neutron-gas density is increased. The curves labeled $n = 20$ correspond to free-space ^{28}O nucleus. As the external neutron-gas density is increased the bound system swells up in a way similar to a density scaling $\rho(r) \rightarrow \rho(sr)$ with $s < 1$ as discussed in Ref. [24]. While the peak of the total density decreases from the free-space value of 0.16 fm^{-3} to as low as 0.068 fm^{-3} for the 1000 external neutron-gas state case, the tail region flattens and develops a larger spatial extent, since the total integral remains to be 28. The density profiles are symmetric about $x = 0$ and the numerical box extends to larger values then shown in the figure. Using these densities in Eq. (4) we have calculated the corresponding ion-ion folding potentials as well as the Coulomb potential. In Fig. 3 these potentials are plotted for a range of external neutron-gas densities. What is observed is that for neutron-gas densities in the range $\rho_{gas} = 2 - 4 \times 10^{12}$ gm/cm^3 the effect of the gas is not changing the ion-ion potential in comparison to the free-space case in a considerable way.
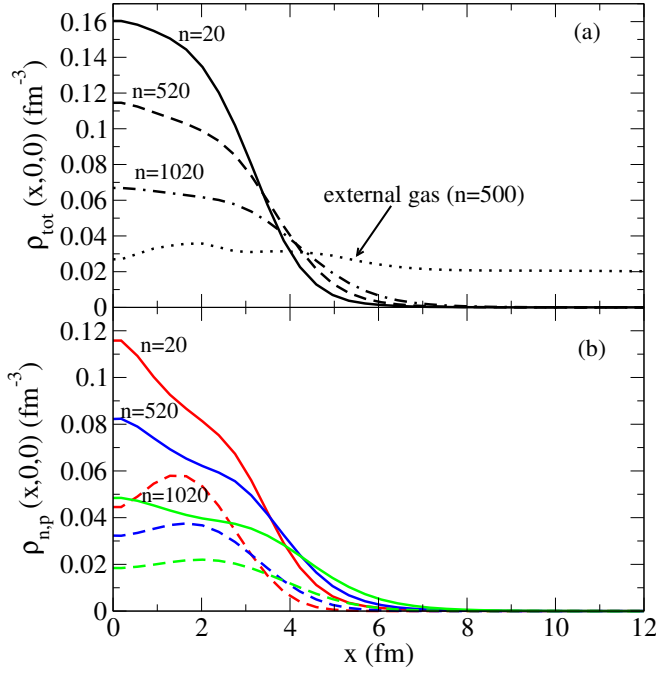
4

FIG. 2. (Color online) (a) Total density profiles for bound states; (b) density profiles for bound neutrons (solid lines) and protons (dashed lines), for the system with $Z = 8$ and $n = 20, 520,$ and 1020 neutrons.
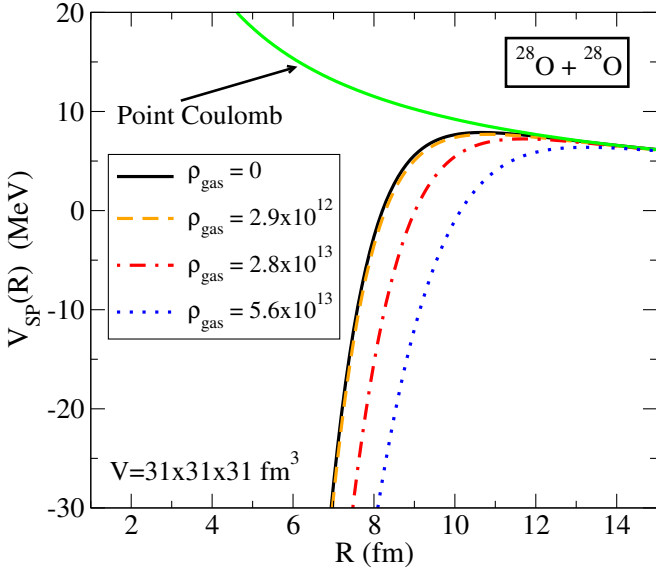

FIG. 3. (Color online) Ion-Ion potentials $V_{SP}(R) = V_F(R) + V_C(R)$ for ^{28}O isotope as a function of the external neutron-gas density. Also shown is the point-Coulomb interaction. Densities are in units of gm/cm^3.

However, for gas densities above 10^{13} gm/cm^3 a very significant change is observed. The free-space barrier has a peak value of 7.87 MeV located at $R = 10.7$ fm. As the external gas density is increased the corresponding barrier height is reduced to 7.69, 7.23, and 6.39 MeV
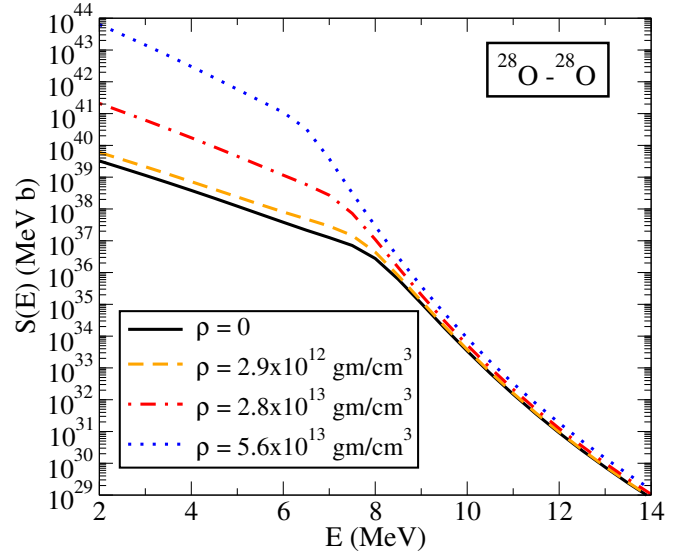

FIG. 4. (Color online) Astrophysical S factor versus center of mass energy for fusion of ^{28}O isotope as a function of external neutron-gas density. Cross-sections are calculated using the São Paulo barriers and the IWBC method.

with the peak location moving outward at 10.8, 11.7, and 13.3 fm. This behavior is very similar to what is observed in free-space as one goes up in the oxygen isotope chain [25]. Unfortunately, the dynamical density constrained time-dependent Hartree-Fock (DC-TDHF) method [26–28] used in Ref. [25] is not applicable in this situation since it requires a fully dynamical calculation.

These together with the calculation of the energy dependence from Eq. (5) allows the calculation of fusion cross-sections as a function of external neutron-gas density, using the IWBC method discussed in the previous section. Figure 4 demonstrates the effect of neutron-gas seen in the potentials on the astrophysical S factor. The S-factor for different external neutron-gas densities start to deviate from each other as soon as the center-of-mass energy falls below the barrier. Even for the lowest gas density of 2.9×10^{12} gm/cm^3 the difference with the free-space value is about a factor of two at the center-of-mass energy of 2 MeV. The difference at higher gas densities are about $1 - 3$ orders of magnitude larger then the free-space values at sub-barrier energies.

In Fig. 5 we plot the cross-sectional density ($y = 0$ plane) profile of the ^{28}O+500n system. In general we see a higher gas density in the vicinity of the nucleus as can also be seen as the dotted line in Fig. 2(a). The energy of this low density neutron gas is so low that even very small "shell effects" can lead to nonuniform densities. In some of the cases we studied the neutron density is low enough to have shell structures leading to the formation of neutron arms seen in Fig. 5. If we replicate this cubic box in three-dimensions one sees a lattice like structure linked by these neutron arms. These effects are driven mainly by the periodic boundary conditions here. Irregularities in the grid of nuclei will produce more irregular
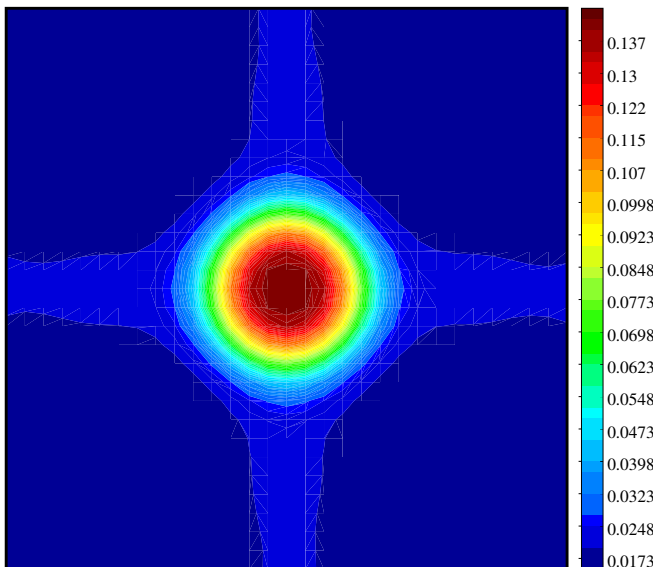
FIG. 5. (Color online) The cross-sectional density ($y = 0$ plane) profile of the ^{28}O+500n system. The neutron density is low enough to have shell structures leading to the formation of neutron arms.
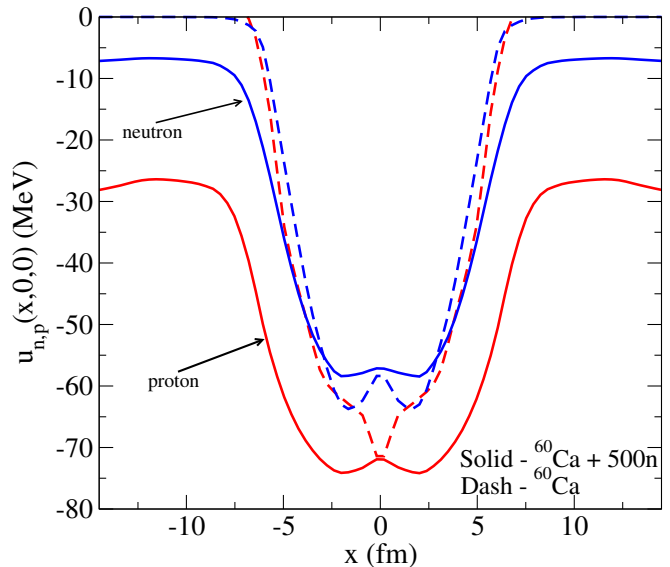

FIG. 6. (Color online) Mean-field potentials for neutrons and protons (solid lines) for the system with $Z = 20$ and 540 neutrons. The dashed lines show the mean-field potential of ^{60}Ca in free-space.

structures of these arms. Since the density in the arms is of the order of free density such that they do not affect the analysis of the bound part.

B. $Z = 20$ system

We have repeated the same study by starting with 20 proton states and a number of neutron states ranging from $140 - 1040$. Using the Skyrme SLy4 we get ^{60}Ca as the slightly bound drip-line nucleus in free-space. For the above range of neutron states we also find the ^{60}Ca to be the bound part of the system. As the number of neutron states is increased an overall negative potential is developed permeating the entire box. Figure 6 shows the neutron and proton mean-field potentials (solid lines) for $Z = 20$ and 540 neutrons. The dashed lines show the mean-field potentials in free-space. In this case the asymptotic value of the neutron potential is about -6.5 MeV. At higher neutron densities we do observe the tendency for ^{72}Ca to be the drip-line nucleus but the tendency is very weak and for practical purposes considering ^{60}Ca is sufficient for the general purposes of this study.

In Fig. 7 we plot the density profiles for neutrons and protons as well as the total density as a function of the number of neutron-gas states. The top frame shows the total density behavior as the neutron-gas density is increased. The curves labeled $n = 40$ correspond to free-space ^{60}Ca nucleus. As the external neutron-gas density is increased the bound system swells up as in the $Z = 8$ case. While the peak of the total density decreases from the free-space value of 0.165 fm^{-3} to as low

as 0.048 fm^{-3} for the 1000 external neutron-gas state case, the tail region flattens and develops a larger spatial extent, since the total integral remains to be 60. The density profiles are symmetric about $x = 0$ and the numerical box extends to larger values then shown in the figure. Corresponding ion-ion folding potentials calculated by using these densities in Eq. (4) are plotted in Fig. 8 for a range of external neutron-gas densities. Again what we observe is that for neutron-gas densities in the range $\rho_{gas} = 2 - 4 \times 10^{12}$ gm/cm^3 the effect of the gas in changing the ion-ion potential compared to the free-space case is not significant. However, for gas densities above 10^{13} gm/cm^3 a very significant change is observed. The free-space barrier has a peak value of 47.4 MeV located at $R = 11.3$ fm. As the external gas density is increased the corresponding barrier height is reduced to 46.3, 42.9, and 37.4 MeV with the peak location moving outward at 11.6, 12.5, and 14.3 fm. Figure 9 shows the fusion cross-sections calculated using the ion-ion potentials shown in Fig. 8. The dramatic rise of the cross-section is obvious as the neutron gas density becomes significantly higher than the minimum neutron drip density.

IV. SUMMARY AND DISCUSSION

To date almost all fusion cross-section calculations done for reactions relevant to the neutron star crust have been done using the São-Paulo folding potential using frozen densities obtained from HF, HFB, or RMF calculations, and without any background of neutrons. Naturally, the environment in which these reactions take place are much more feature rich depending on the location in
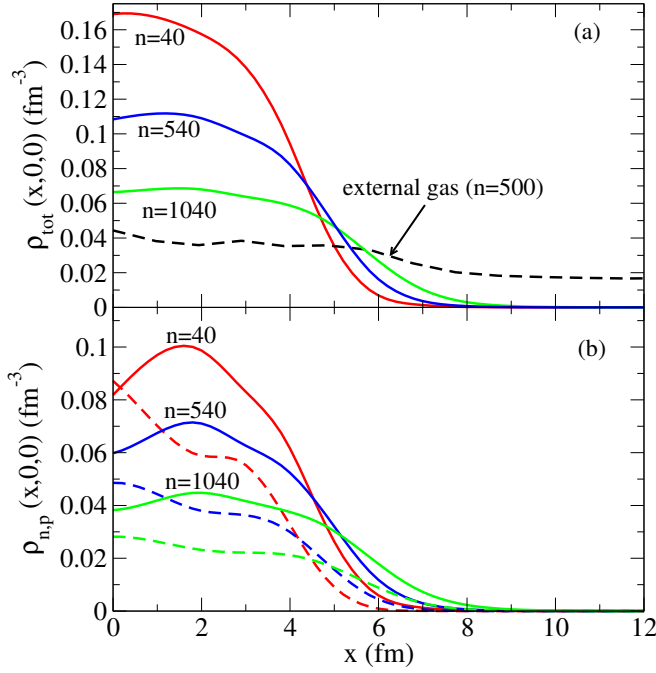
FIG. 7. (Color online) (a) Total density profiles for bound states; (b) density profiles for bound neutrons (solid lines) and protons (dashed lines), for the system with $Z = 20$ and $n = 40, 540,$ and 1040 neutrons.
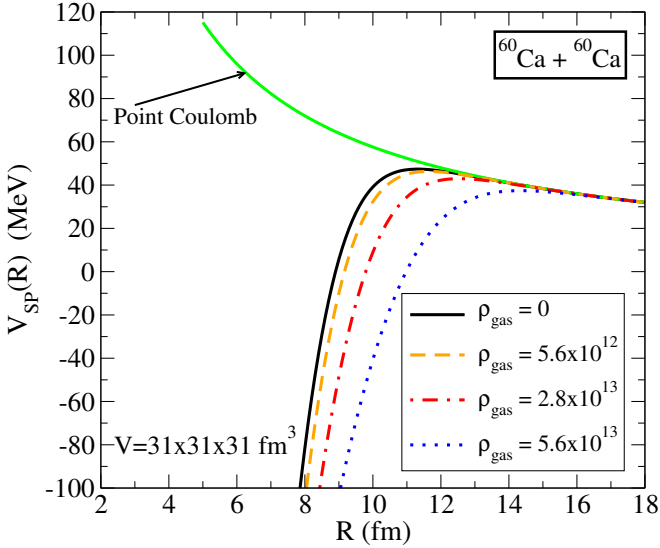

FIG. 8. (Color online) Ion-Ion potentials $V_{SP}(R) = V_F(R) + V_C(R)$ between two ^{60}Ca isotopes as a function of the external neutron-gas density. Also shown is the point-Coulomb interaction. Densities are in units of gm/cm^3.

FIG. 9. (Color online) Fusion cross-section as a function of center-of-mass energy for the fusion of two ^{60}Ca isotopes calculated for changing external neutron-gas density. Cross-sections are calculated using the São Paulo barriers and the IWBC method.

new aspect which we study here is the effect of the presence of a background neutron gas environment on the nuclei in this coexistent phase between the start of the neutron drip region and the melting region. For our study we have used an approach that treats the nuclei and the extra neutrons in a unified manner both packing them into one Slater state for the whole system. The computations are done in full 3D with periodic boundary conditions and a special treatment of the Coulomb potential with periodic boundary conditions. For the calculation of fusion cross-sections we have used the São-Paulo model. In our calculations we observe that for lower background densities the cross-sections do not change in a very significant manner. On the other hand as we increase the neutron gas density we observe the swelling of the nuclei that results in the lowering of the ion-ion potential barriers and significant increase in the fusion cross-sections. At densities higher than the neutron-drip regime the melting of the nuclei can be observed.

One of the major omissions in our approach is the absence of pairing [29–31]. An extended treatment including pairing constitutes the next milestone. Let us, nonetheless, briefly comment on possible pairing effects. First is the pairing interaction influencing the structure of the isolated nuclei. Naturally for the examples studied here we do not have any proton pairing. Pairing interaction could be present among neutrons as we move to neutron rich isotopes. As one approaches the drip-line nuclei the gap becomes smaller and smaller and becomes negligible at the drip line but the presence of pairing can influence the exact location of the drip line (by at most 2 nucleon units) and may also lead to a somewhat larger surface thickness. The primary influence of pairing on fu-

the crust. As the first milestone in incorporating this environment we have investigated pycnonuclear reactions which are expected to occur between very neutron-rich nuclei in a background of a neutron gas [10]. Here we focused on the neutron drip region of the inner crust where most nuclei are expected to be on the drip line. The basic
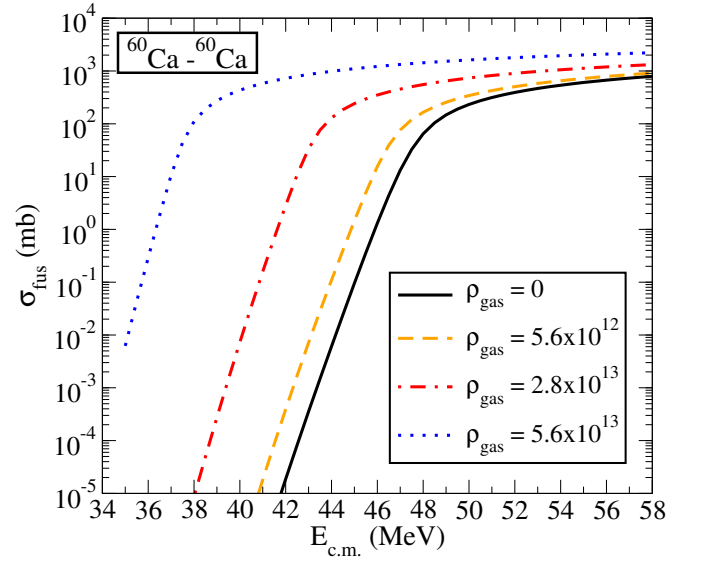
sion within the folding-potential model is related to the initial structure of the nucleus. However, for light nuclei, considered for the inner crust, the pairing effects are expected to be small. The inclusion of pairing for the combined system of a neutron gas and embedded nuclei is somewhat more involved. Neutron matter at typical densities for the inner crust is believed to show an s-wave neutron superfluidity [32–38] with a gap of 1-2.5 MeV depending on the used model. Perturbation by an immersed nucleus will reduce superfluidity in its vicinity. However, we cannot exclude that superfluidity further away in the surrounding neutron background may influence the dynamics of fusion in this region in a fully dynamical calculation. Still, we expect the general observation of the swelling of nuclear density to behave similar to the results obtained in this study.

Besides the pairing issue, calculation of fusion using frozen densities is in itself a serious approximation. In recent past we have used the DC-TDHF approach to actually use dynamical densities, including neck formation and transfer, to calculate such cross-sections [25] relevant for the neutron star crust. As it was shown the deformation effects and dynamics does influence the sub-barrier fusion cross-sections. However, some of these effects are phenomenologically contained through the energy dependence of the São-Paulo potential. Unfortu-

nately, at this stage the numerical and conceptual issues prevent us from using the DC-TDHF method in the presence of the neutron gas background. However, work is on the way to study the dynamics of nuclei moving inside the neutron gas.

It is clear from the above discussion that a fully dynamical study of fusion in the presence of the full environment and with the inclusion of pairing is the desirable goal. In a dynamical calculation the movement of nuclei may cause ripples and waves in the neutron background that can also influence these results. However, in the adiabatic limit these effects are not expected to be very large. While our methods give us a good understanding of fusion under these conditions more precise computations, including the full effects of pairing and effective interactions tailored for neutron star crust [39], may reduce some of the observed shell effects and modify some of the results but the main effects observed here are expected to remain the same.

[1] A. B. Balantekin, J. Carlson, D. J. Dean, G. M. Fuller, R. J. Furnstahl, M. Hjorth-Jensen, R. V. F. Janssens, Bao-An Li, W. Nazarewicz, F. M. Nunes, W. E. Ormand, S. Reddy, and B. M. Sherrill, "Nuclear theory and science of the facility for rare isotope beams," Mod. Phys. Lett. A **29**, 1430010 (2014).

[2] P. Haensel, A.Y. Potekhin, and D.G. Yakovlev, *Neutron Stars 1:Equation of State and Structure* (Springer-Verlag, New York, 2007).

[3] H. Schatz, A. Aprahamian, V. Barnard, L. Bildsten, A. Cumming, M. Ouellette, T. Rauscher, F. K. Thielemann, and M. Wiescher, "End point of the rp process on accreting neutron stars," Phys. Rev. Lett. **86**, 3471–3474 (2001).

[4] Sanjib Gupta, Edward F. Brown, Hendrik Schatz, Peter Möller, and Karl-Ludwig Kratz, "Heating in the accreted neutron star ocean: Implications for superburst ignition," Astrophys. J. **662**, 1188–1197 (2007).

[5] E. E. Salpeter and H. M. Vanhorn, "Nuclear reaction rates at high densities," Astrophys. J. **155**, 183 (1969).

[6] S. Schramm and S. E. Koonin, "Pycnonuclear fusion rates," Astrophys. J. **365**, 296–300 (1990).

[7] J.W. Negele and D. Vautherin, "Neutron star matter at sub-nuclear densities," Nuclear Physics A **207**, 298 – 320 (1973).

[8] C. J. Horowitz, H. Dussan, and D. K. Berry, "Fusion of neutron-rich oxygen isotopes in the crust of accreting neutron stars," Phys. Rev. C **77**, 045807 (2008).

[9] M. Beard, A. V. Afanasjev, L. C. Chamon, L. R. Gasques, M. Wiescher, and D. G. Yakovlev, "Astrophysical s factors for fusion reactions involving c, o, ne, and

mg isotopes," Atomic data and nuclear data tables **96**, 541–566 (2010).

[10] A. V. Afanasjev, M. Beard, A. I. Chugunov, M. Wiescher, and D. G. Yakovlev, "Large collection of astrophysical s factors and their compact representation," Phys. Rev. C **85**, 054615 (2012).

[11] A. S. Umar and V. E. Oberacker, "Three-dimensional unrestricted time-dependent hartree-fock fusion calculations using the full skyrme interaction," Phys. Rev. C **73**, 054607 (2006).

[12] J. A. Maruhn, P.-G. Reinhard, P. D. Stevenson, and A. S. Umar, "The tdhf code sky3d," Comp. Phys. Comm. **185**, 2195–2216 (2014).

[13] A. S. Umar, M. R. Strayer, J. S. Wu, D. J. Dean, and M. C. Güçlü, "Nuclear hartree-fock calculations with splines," Phys. Rev. C **44**, 2512–2521 (1991).

[14] A. S. Umar, J. Wu, M. R. Strayer, and C. Bottcher, "Basis-spline collocation method for the lattice solution of boundary-value-problems," J. Comp. Phys. **93**, 426–448 (1991).

[15] C. Bottcher, M. R. Strayer, A. S. Umar, and P.-G. Reinhard, "Damped relaxation techniques to calculate bound-states," Phys. Rev. A **40**, 4182–4189 (1989).

[16] E. Chabanat, P. Bonche, P. Haensel, J. Meyer, and R. Schaeffer, "A skyrme parametrization from subnuclear to neutron star densities - part ii. nuclei far from stabilities," Nucl. Phys. A **635**, 231–256 (1998).

[17] F. Douchin and P. Haensel, "A unified equation of state of dense matter and neutron star structure," Astron. Astrophys. **380**, 151–167 (2001).

[18] L. R. Gasques, L. C. Chamon, D. Pereira, M. A. G. Alvarez, E. S. Rossi, C. P. Silva, and B. V. Carlson, "Global and consistent analysis of the heavy-ion elastic scattering and fusion processes," Phys. Rev. C **69**, 034603 (2004).

[19] L. C. Chamon, B. V. Carlson, L. R. Gasques, D. Pereira, C. De Conti, M. A. G. Alvarez, M. S. Hussein, M. A. C. Ribeiro, E. S. Rossi, and C. P. Silva, "Toward a global description of the nucleus-nucleus interaction," Phys. Rev. C **66**, 014610 (2002).

[20] L. R. Gasques, A. V. Afanasjev, E. F. Aguilera, M. Beard, L. C. Chamon, P. Ring, M. Wiescher, and D. G. Yakovlev, "Nuclear fusion in dense matter: Reaction rate and carbon burning," Phys. Rev. C **72**, 025806 (2005).

[21] L. R. Gasques, A. V. Afanasjev, M. Beard, J. Lubian, T. Neff, M. Wiescher, and D. G. Yakovlev, "São paulo potential as a tool for calculating s factors of fusion reactions in dense stellar matter," Phys. Rev. C **76**, 045802 (2007).

[22] D. G. Yakovlev, M. Beard, L. R. Gasques, and M. Wiescher, "Simple analytic model for astrophysical s factors," Phys. Rev. C **82**, 044609 (2010).

[23] K. Hagino, N. Rowley, and A. T. Kruppa, "A program for coupled-channel calculations with all order couplings for heavy-ion fusion reactions," Comput. Phys. Commun. **123**, 143–152 (1999).

[24] A. S. Umar and V. E. Oberacker, "Compressibility and equation of state of finite nuclei," Phys. Rev. C **76**, 024316 (2007).

[25] A. S. Umar, V. E. Oberacker, and C. J. Horowitz, "Microscopic sub-barrier fusion calculations for the neutron star crust," Phys. Rev. C **85**, 055801 (2012).

[26] A. S. Umar and V. E. Oberacker, "Heavy-ion interaction potential deduced from density-constrained time-dependent hartree-fock calculation," Phys. Rev. C **74**, 021601 (2006).

[27] A. S. Umar, V. E. Oberacker, and J. A. Maruhn, "Neutron transfer dynamics and doorway to fusion in time-dependent hartree-fock theory," Eur. Phys. J. A **37**, 245–250 (2008).

[28] R. Keser, A. S. Umar, and V. E. Oberacker, "Microscopic study of ca plus ca fusion," Phys. Rev. C **85**, 044606 (2012).

[29] J. Dobaczewski, W. Nazarewicz, T. R. Werner, J. F. Berger, C. R. Chinn, and J. Decharge, "Mean-field description of ground-state properties of drip-line nuclei: Pairing and continuum effects," Phys. Rev. C **53**, 2809–2840 (1996).

[30] F. Montani, C. May, and H. Müther, "Mean field and pairing properties in the crust of neutron stars," Phys. Rev. C **69**, 065801 (2004).

[31] J. R. Stone, J. C. Miller, R. Koncewicz, P. D. Stevenson, and M. R. Strayer, "Nuclear matter and neutron-star properties calculated with the skyrme interaction," Phys. Rev. C **68**, 034324 (2003).

[32] D. Ding, A. Rios, W. H. Dickhoff, H. Dussan, A. Polls, and S. J. Witte, "Pairing in high-density neutron matter including short- and long-range correlations," arXiv:1502.05673 (2015).

[33] S. Gandolfi, A. Yu. Illarionov, F. Pederiva, K. E. Schmidt, and S. Fantoni, "Equation of state of low-density neutron matter, and the $^1S_0$ pairing gap," Phys. Rev. C **80**, 045802 (2009).

[34] D. J. Dean and M. Hjorth-Jensen, "Pairing in nuclear systems: from neutron stars to finite nuclei," Rev. Mod. Phys. **75**, 607–656 (2003).

[35] M. Baldo, E.E. Saperstein, and S.V. Tolokonnikov, "Superfluidity in nuclear and neutron matter," Nuclear Physics A **749**, 42 – 52 (2005).

[36] Aurel Bulgac, "Local density approximation for systems with pairing correlations," Phys. Rev. C **65**, 051305 (2002).

[37] Aurel Bulgac and Yongle Yu, "Renormalization of the hartree-fock-bogoliubov equations in the case of a zero range pairing interaction," Phys. Rev. Lett. **88**, 042504 (2002).

[38] Aurel Bulgac, Michael McNeil Forbes, and Shi Jin, "Nuclear energy density functionals: What do we really know?" arXiv:1506.09195 (2015).

[39] J. Erler, C. J. Horowitz, W. Nazarewicz, M. Rafalski, and P.-G. Reinhard, "Energy density functional for nuclei and neutron stars," Phys. Rev. C **87**, 044320 (2013).